SUPPLEMENTARY INFORMATION

Flexible Organic-Inorganic Hybrid Crystals of Tin(IV) Chloride and Naphthalenediimide: Exploring Elasticity, Mechanochromism, and Photothermal Conversion

Sotaro Kusumoto,*[a] Shunya Masuda,[a] Ryo Suzuki,[b] Masaru Tachibana,[b] Masaya Shimabukuro,[c] Mamiko Kobayashi,[c] Naoki Ogiwara,[d] Sayaka Uchida,[d] Tomoya Fukui,[e] Yuta Tsuji,[f] Masaya Okamura,[a] Shiro Hikichi,[a] Yang Kim,[g] Yoshihiro Koide*[a]

[a] Dr. S. Kusumoto, Mr. S. Masuda, Dr. M. Okamura, Prof. Dr. S. Hikichi, Prof. Dr. Y. Koide
Department of Applied Chemistry, Faculty of Chemistry and Biochemistry, Kanagawa University, 3-27-1 Rokkakubashi, Kanagawa-ku, Yokohama 221-8686, Japan.
E-mail: kusumoto@kanagawa-u.ac.jp, ykoide01@kanagawa-u.ac.jp
[b] Dr. R. Suzuki, Prof. Dr. M. Tachibana
Department of Materials System Science, Yokohama City University, 22-2 Seto, Kanazawa-ku, Yokohama, Kanagawa 236-0027, Japan.
[c] Dr. Shimabukuro, M. Kobayashi
Institute of Biomaterials and Bioengineering, Tokyo Medical and Dental University, 2-3-10, Kanda-Surugadai, Chiyoda-ku, Tokyo 101-0062, Japan.
[d] Dr. N. Ogiwara, Prof. Dr. S. Uchida
Department of Basic Science, School of Arts and Sciences, The University of Tokyo, 3-8-1 Komaba, Meguro, Tokyo 153-0041, Japan.
[e] Dr. T. Fukui
Laboratory for Chemistry and Life Science, Institute of Integrated Research, Institute of Science Tokyo, 4259 Nagatsuta-cho, Midori-ku, Yokohama, Kanagawa 226-8501, Japan.
[f] Dr. Y. Tsuji
Faculty of Engineering Sciences, Kyushu University, Kasuga, Fukuoka 816-8580, Japan
[g] Prof. Dr. Y. Kim
Department of Chemistry, Graduate School of Science and Technology, Kumamoto University, 2-39-1 Kurokami, Chuo-ku, Kumamoto 860-8555, Japan.

Table S1. Crystallographic data of **1w** and **1**.

Compound	**1w**	**1**
formula	$C_{52}\ H_{42}\ Cl_{12}\ N_8\ O_{11}\ Sn_2$	$C_{26}\ H_{18}\ Cl_6\ N_4\ O_4\ Sn$
formula weight	1617.71	781.83
crystal system	monoclinic	monoclinic
space group	$P2_1/c$	$P2_1/c$
a / Å	16.2608(5)	8.2116(2)
b / Å	16.4969(5)	24.2462(7)
c / Å	23.1911(7)	14.1698(4)
α / º	90	90
β / º	103.600(3)	100.268(3)
γ / º	90	90
V / Å^3	6046.6(3)	2776.03(13)
Z	4	4
T / K	120	120
R_1	0.0461	0.0290
R_1 (all data)	0.0682	0.0418
wR_2	0.0929	0.0617
wR_2 (all data)	0.1048	0.0653
G.O.F.	1.039	1.053
CCDC	2417348	2417349

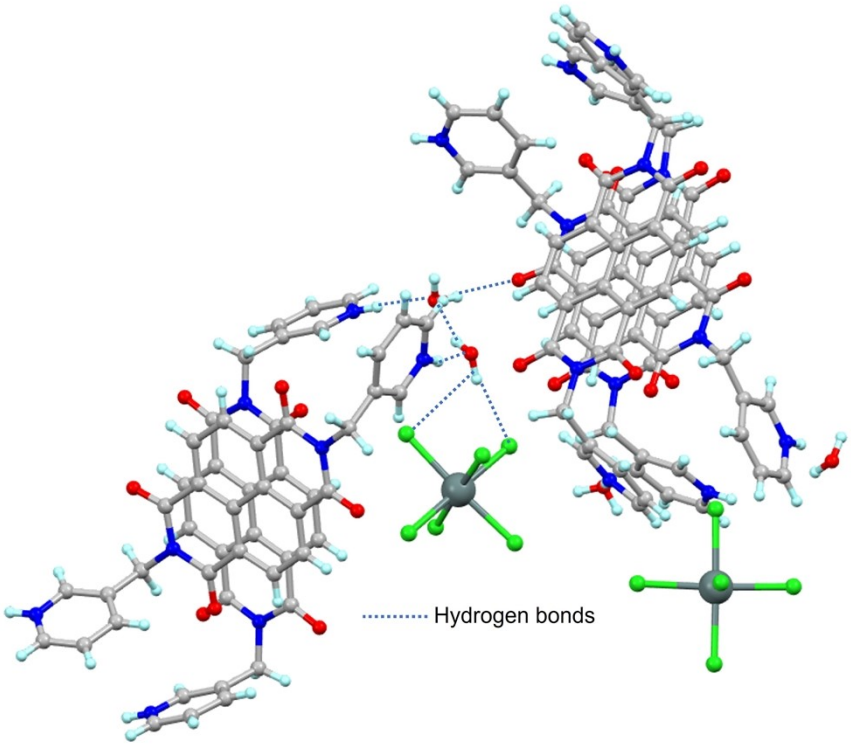

Figure S1 Hydrogen Bonding around water molecules in crystal **1w**.

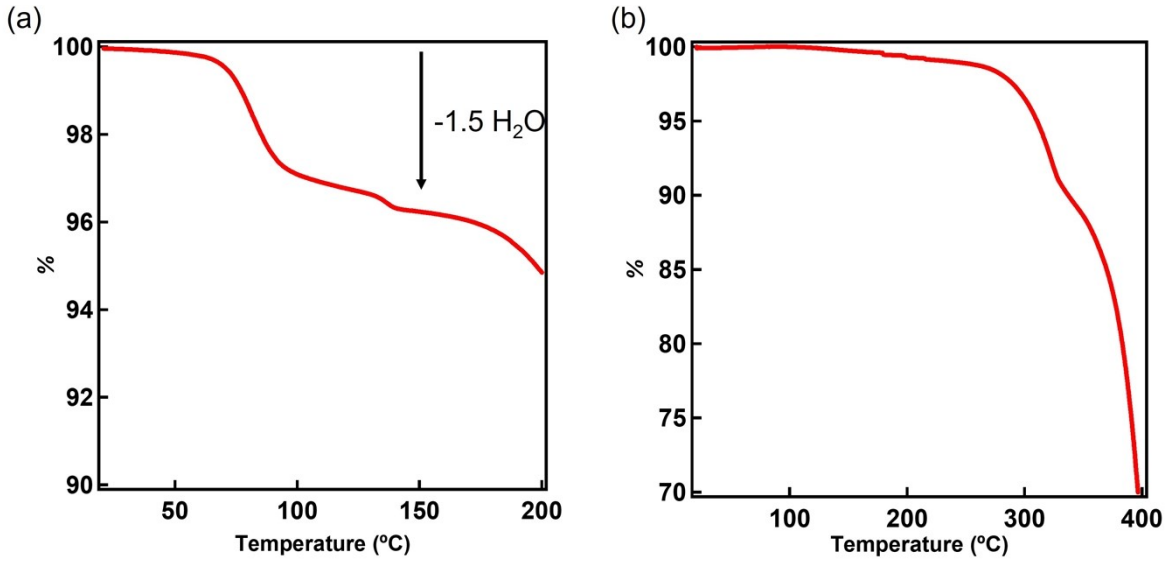

Figure S2 Thermogravimetric analysis (TGA) for **1w** (a) and **1** (b).

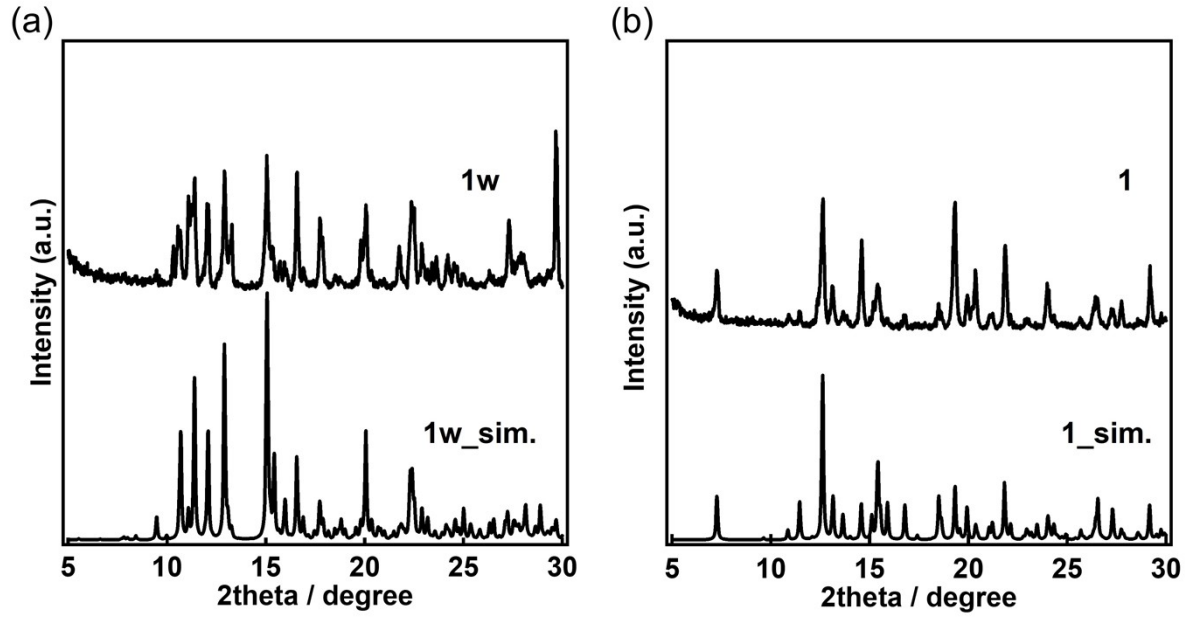

Figure S3 Powder X-ray diffraction (PXRD) patterns of the as-synthesized samples **1w** (a) and **1** (b).

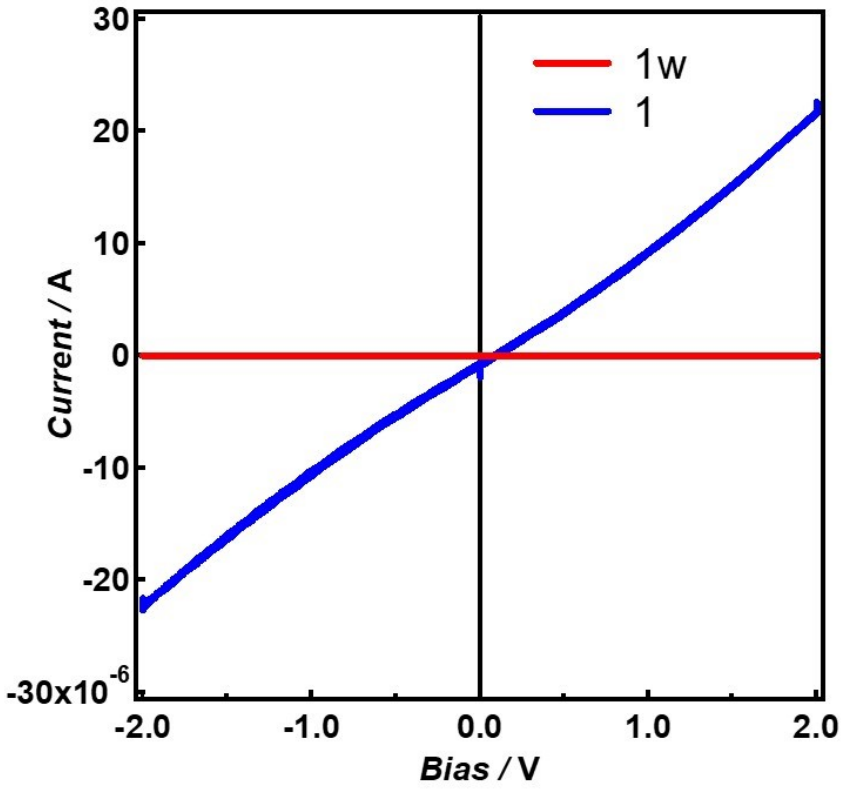

Figure S4 Electrical conductivity measurements of **1w** and **1** pellets.

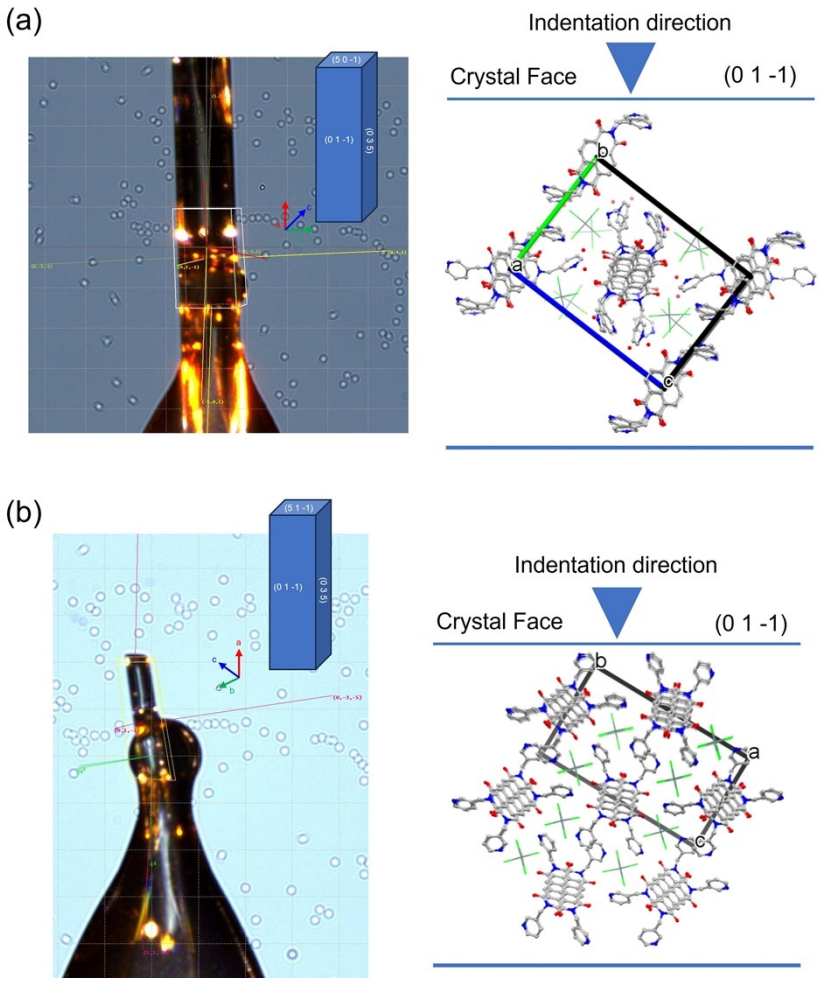

Figure S5 Face index results for **1w** (a) and **1** (b), along with the indentation directions in nanoindentation and their corresponding crystal structures.

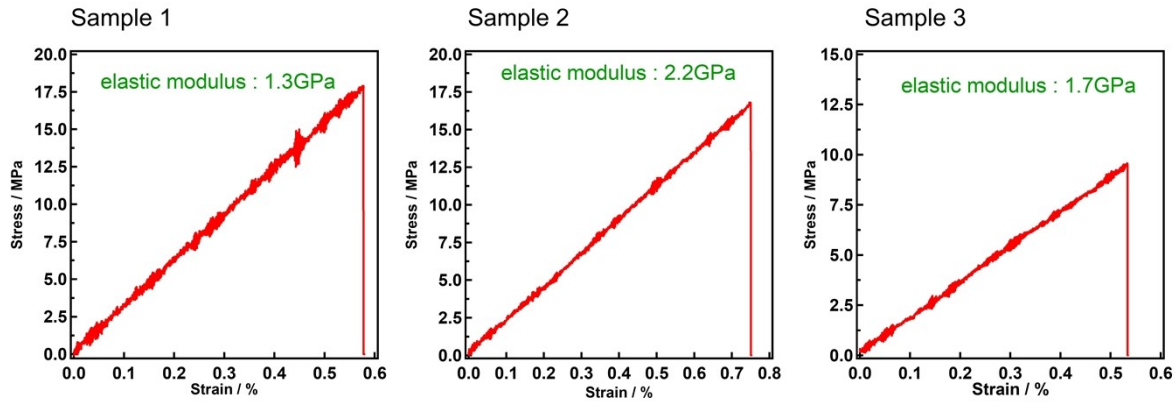

	Width (mm)	Thickness (mm)	Elastic Modulus (GPa)
Sample 1	0.189	0.202	1.3
Sample 2	0.228	0.217	2.2
Sample 3	0.296	0.242	1.7

Figure S6 Stress-strain curves from the three-point bending test of the 1w crystal, along with a table outlining the thickness and width of each crystal.

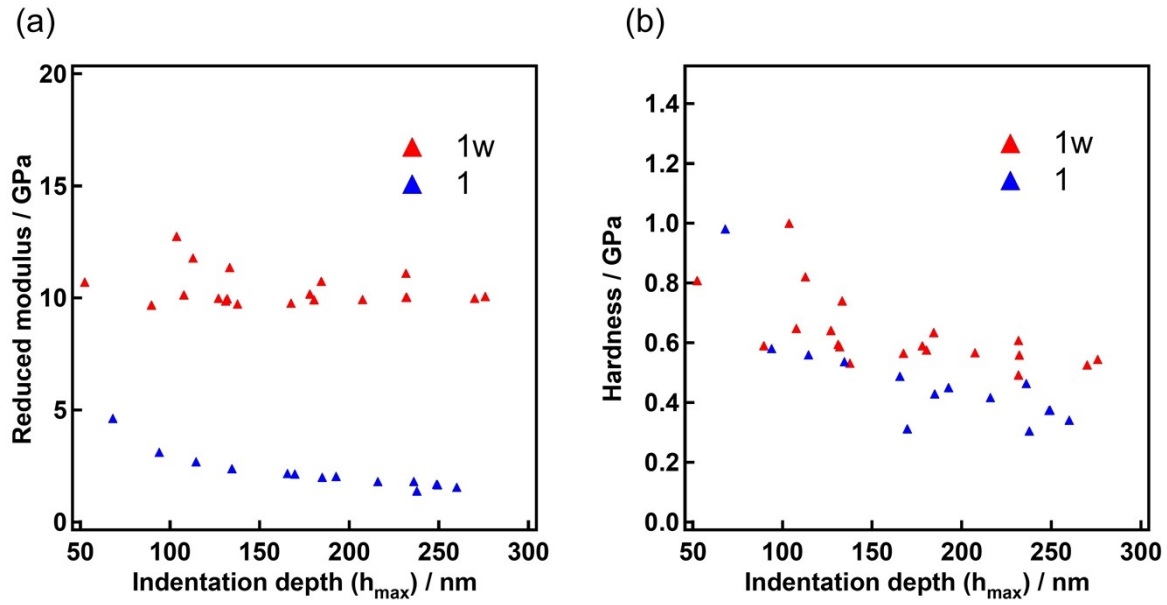

Figure S7 Depth dependence of the reduced modulus (a) and hardness (b) for **1w** and **1**.

Table S2 Table of elastic moduli obtained from three-point bending tests on selected elastic crystals.

Compounds	Elastic Modulus (GPa)
MMIAB[1]	1.3
BTP[2]	1.6
1w	**2.3**
CXC[3]	2.41
P-2[4]	2.45
OXB[3]	3.24
P-1[4]	3.51
BZC[3]	3.56
EHMAPA[5]	3.73
BZF[3]	4.33
BZB[3]	5.51
DMPIN[6]	6.0
EC3[7]	6.07
Cu(acac)$_2$[8]	8.0

EC2[7]	8.95

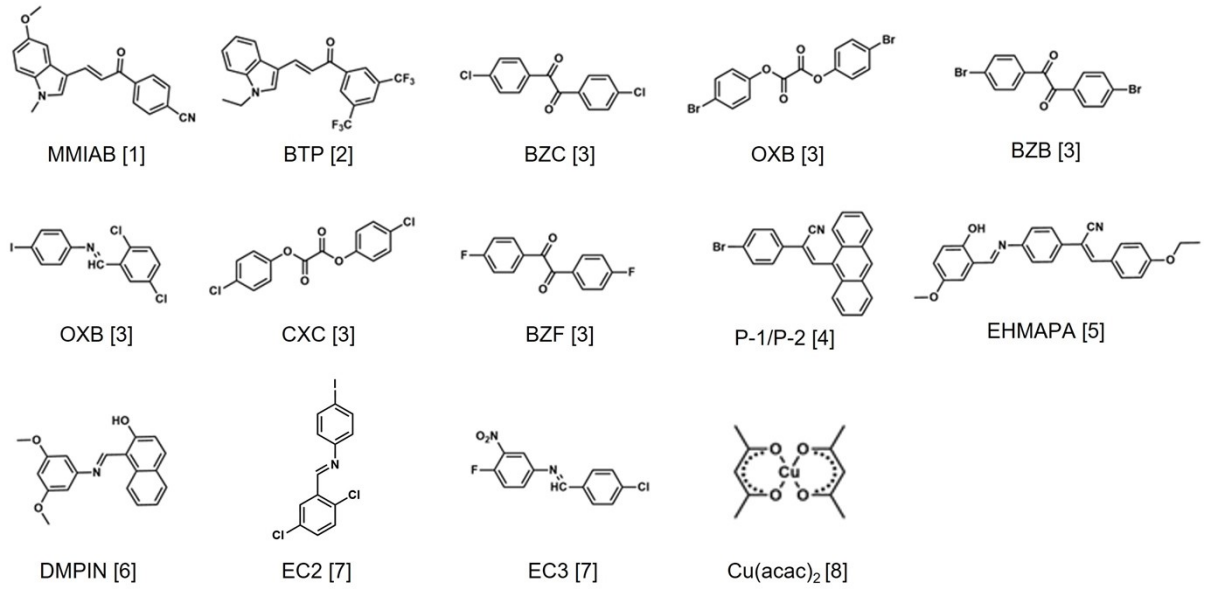

Table S3 Table displaying the reduced moduli (*E*r) and hardness (*H*) values obtained from nanoindentation tests of selected reported elastic organic and metal complex crystals.

Compounds	E_r (GPa)	*h* (GPa)
1	**1.84**	**0.40**
$Cu(acac)_2$ (101) [8]	4.8	0.20
TDD[9]	5.37	0.13
DPZ[10]	5.83	0.26
Terpy-N (001) [11]	7.5	0.45
EC3[7]	8.4	0.29
Terpy-A (001) [11]	9.3	0.75
1w	**10.6**	**0.59**
$Cu(acac)_2$ ($10\bar{1}$) [8]	11.3	0.38
EC4[7]	12.5	0.37
EC2[7]	12.8	0.23

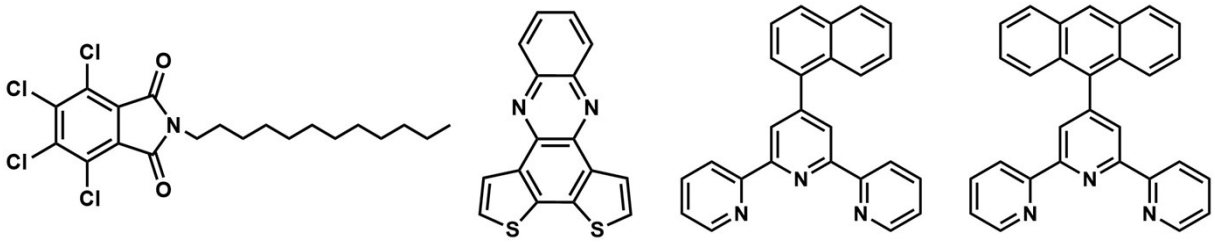

TDD [9] DPZ [10] Terpy-N [11] Terpy-A [11]

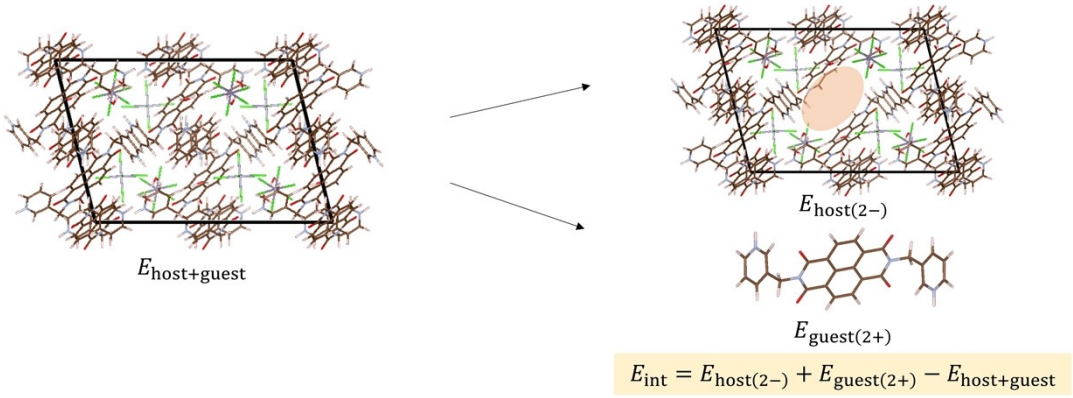

1w	$E_{\text{host+guest}}$	$E_{\text{host(2-)}}$	$E_{\text{guest(2+)}}$	E_{int}
E_{tot} (eV)	-3287.33	-2916.44	-351.249	19.6458
E_{disp} (eV)	-33.9537	-28.7735	-0.97366	4.20652

1	$E_{\text{host+guest}}$	$E_{\text{host(2-)}}$	$E_{\text{guest(2+)}}$	E_{int}
E_{tot} (eV)	-1554.33	-1184.15	-351.275	18.9102
E_{disp} (eV)	-16.8237	-11.8165	-0.95835	4.04883

Figure S8 Results of calculations on intermolecular interaction energies using DFT. Results of calculations on intermolecular interaction energies using DFT. $E_{\text{host(2-)}}$ and $E_{\text{guest(2+)}}$ were calculated using unit cells charged with -2 and +2, respectively. E_{tot} and E_{disp} represent the total energy of the system and the energy contribution from the dispersion correction, respectively.

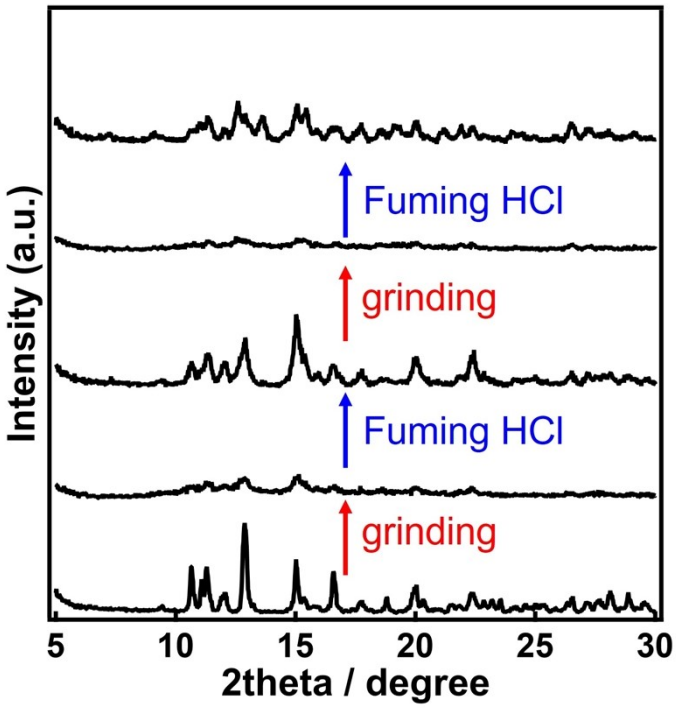

Figure S9 Repeatability of the mechanochromism of **1w** in PXRD.

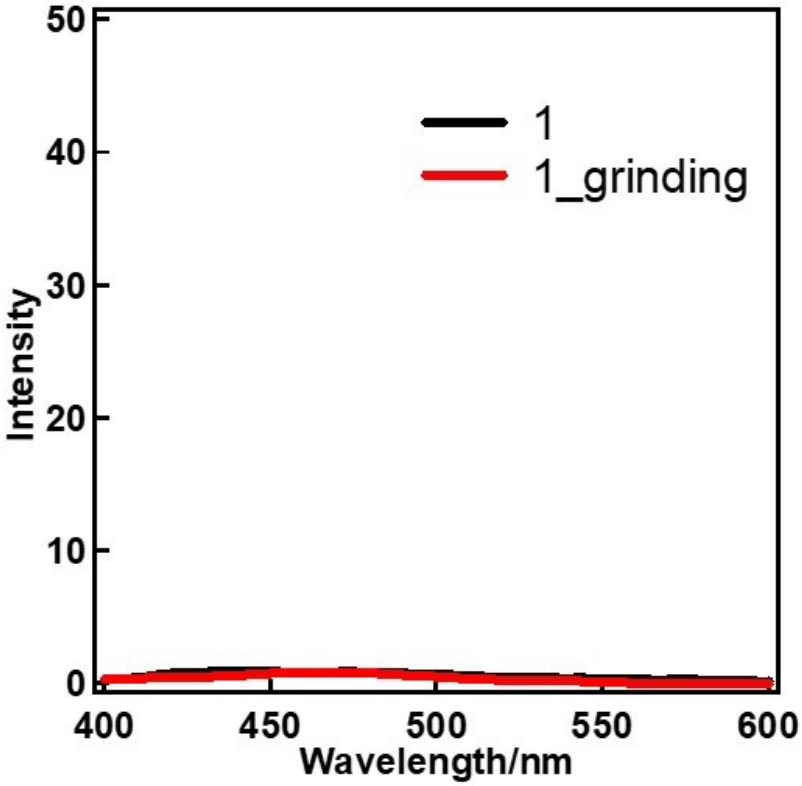

Figure S10 Emission spectra (λ_{ex} =350 nm) of **1** before and after grinding.

Calculation Method for Photothermal Conversion Efficiency (*η*)

The specific heat capacities of **1** was calculated using DSC measurements and Ag_2S (around 0.7 *J*/(g·K)) as the reference material. The specific heat capacity (C_p) is defined as $C_p = Q / (m \times \Delta T)$, where Q is heat (*J*) and m is mass (g). In the temperature range of 40-90 °C, the specific heat capacity of **1** is 1.10-1.39 *J*/(g-K) (Figure S9a). To calculate the thermal conversion efficiency, the average specific heat capacity from 40 to 90 °C (1.26 *J*/(g-K)) was used.

Given the information on absorbance, photothermal temperature, and heat capacity, the rough photothermal conversion efficiency (*η*) can be calculated using the method described in Ref. 38 of the main text.

$$mC_p\frac{\mathrm{d}T}{\mathrm{d}t} = Q_s - Q_{loss}$$

Here, *m* (using 30 mg for **1**) and C_p represent the mass and heat capacity of the solid, respectively, and Q_s is the photothermal energy input from irradiation, expressed by the following equation:

$$Q_s = I(1-R)_{\eta}$$

where *I* is the laser power (0.3 W/cm^{-2}), and *R* is the reflectance at the excitation wavelength of 850 nm (Figure S9b). Q_{loss} is the thermal energy lost to the surroundings, which is approximately proportional to the linear thermal driving force:

$$Q_{loss} = hS(T - T_{surr})$$

where *h* is the heat transfer coefficient, *S* is the surface area of the container, and T_{surr} is the ambient temperature. When the temperature reaches its maximum, the system reaches equilibrium (Figure S9c). Thus,

$$Q_s - Q_{loss} = hS(T_{max} - T_{surr})$$

(T_{max} - T_{surr}) is 84.3 K for **1**. The conversion efficiency *η* is calculated as:

$$\eta = \frac{hS(T_{max} - T_{surr})}{I(1-R)}$$

To determine *hS*, we introduce the dimensionless driving force ϑ as follows:

$$\theta = \frac{T - T_{surr}}{T_{max} - T_{surr}}$$

Derive θ with respect to *T* and we get

$$\frac{d\theta}{dt} = -\frac{Q_s}{mC_p(T_{max} - T_{surr})} - \frac{hs\theta}{mC_p}$$

When the laser is off, $Q_s = 0$, thus:

$$\frac{d\theta}{dt} = -\frac{hs\theta}{mC_p}$$

Integrating, we get:

$$t = -\frac{mC_p}{hs} ln\theta$$

Therefore, *hS* can be calculated from the slope of the cooling time vs. ln ϑ plot (Figure S9d). *hS* is found to be 4.2808×10^{-4} J/(Ks) for **1**. According to the equation, the conversion efficiency η for **1** is finally calculated to be 63%.

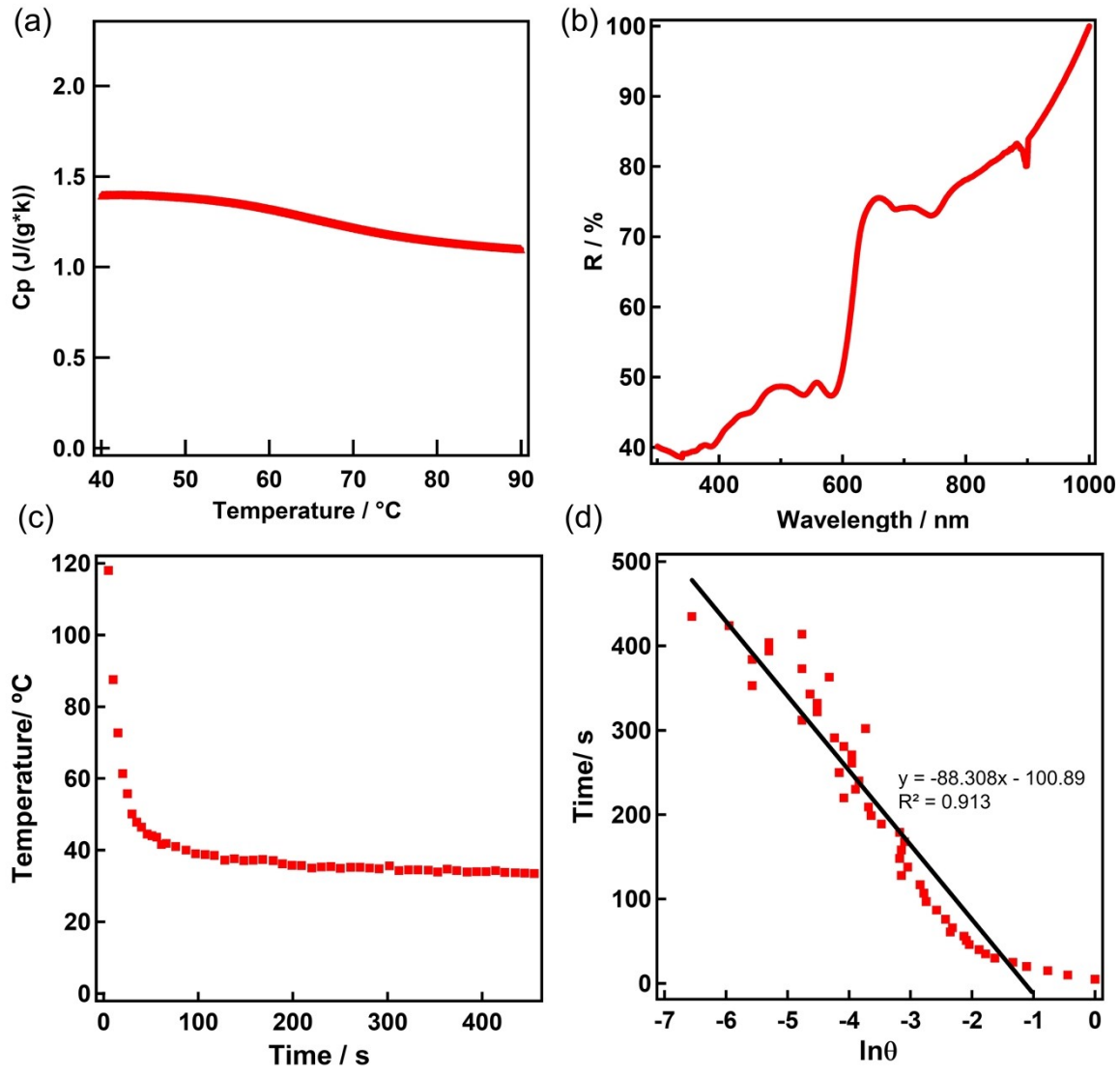

Figure S11 (a) Specific heat capacity of **1**, measured from 40 to 90 °C. (b) UV-Vis-NIR diffused reflectance

spectra of **1**. (c) The cooling curve of **1** after irradiating with 850 nm laser (0.3 W cm^{-2}) (c), along with its corresponding time-ln(ϑ) linear curve (d).

References

1) Q. Di, J. Li, Z. Zhang, X. Yu, B. Tang, H. Zhang, and H. Zhang, *Chem. Sci*., 2021, **12**, 15423–15428.
2) Q. Di, L. Li, X. Miao, L. Lan, X. Yu, B. Liu, Y. Yi, P. Naumov, and H. Zhang, *Nat. Commun*., 2022, **13**, 5280.
3) I. S. Divya, S. Kandasamy, S. Hasebe, T. Sasaki, H. Koshima, K. Woźniak, and S. Varughese, *Chem. Sci*., 2022, **13**, 8989-9003.
4) Y. Wei, X. Xu, X. Yang, and H. Zhang, *Cryst. Growth Des*., 2023, **23**, 8204–8211.
5) L. Lan, Q. Di, L. Li, B. Liu, X. Yu, P. Naumov, and H. Zhang, *Cryst. Growth Des*., 2022, **22**, 3435−3441.
6) H. Liu, Z. Lu, B. Tang, C. Qu, Z. Zhang, and H. Zhang, *Angew. Chem. Int. Ed.*, 2020, **59**, 12944–12950.
7) M. K. Mishra, S. B. Kadambi, U. Ramamurty, and S. Ghosh, *Chem. Commun.*, 2018, **54**, 9047-9050.
8) A. Worthy, A. Grosjean, M. C. Pfrunder, Y. Xu, C. Yan, G. Edwards, J. K. Clegg, and J. C. McMurtrie, *Nat. Commun.*, 2018, **10**, 65-69.
9) S. Kusumoto, R. Suzuki, M. Tachibana, Y. Sekine, Y. Kim, S. Hayami, *Chem. Commun.*, 2022, **58**, 5411-5414.
10) M. Annadhasan, A. R. Agrawal, S. Bhunia, V. V. Pradeep, S. S. Zade, C. M. Reddy, R. Chandrasekar, *Angew. Chem. Int. Ed.*, 2020, **59**, 13852–13858.
11) S. Kusumoto, K. Oishi, M. Nakaya, R. Suzuki, M. Tachibana, Y. Kim, Y. Koide, and S. Hayami, *CrystEngComm*, 2022, **24**, 8303-8308.